Temporal complexity of fMRI is reproducible and correlates with higher order cognition

Omidvarnia, Amir; Zalesky, Andrew; Mansour L, Sina; Van De Ville, Dimitri; Jackson, Graeme D.; Pedersen, Mangor

How to cite

OMIDVARNIA, Amir et al. Temporal complexity of fMRI is reproducible and correlates with higher order cognition. In: NeuroImage, 2021, vol. 230, p. 117760. doi: 10.1016/j.neuroimage.2021.117760

This publication URL: https://archive-ouverte.unige.ch/unige:168802
Publication DOI: 10.1016/j.neuroimage.2021.117760

NeuroImage 230 (2021) 117760

Contents lists available at ScienceDirect

NeuroImage

journal homepage: www.elsevier.com/locate/neuroimage

Temporal complexity of fMRI is reproducible and correlates with higher order cognition

Amir Omidvarnia[a,b,f,*], Andrew Zalesky[c,d], Sina Mansour L.[c,d], Dimitri Van De Ville[a,b], Graeme D. Jackson[e,f,g], Mangor Pedersen[f,h]

[a] Institute of Bioengineering, Center for Neuroprosthetics, Center for Biomedical Imaging, EPFL, Lausanne, Switzerland
[b] Department of Radiology and Medical Informatics, University of Geneva, Geneva, Switzerland
[c] Melbourne Neuropsychiatry Centre, Department of Psychiatry, The University of Melbourne, Melbourne, Australia
[d] Department of Biomedical Engineering, The University of Melbourne, Melbourne, Australia
[e] The Florey Institute of Neuroscience and Mental Health, Melbourne Brain Centre, Melbourne, Australia
[f] Florey Department of Neuroscience and Mental Health, The University of Melbourne, Melbourne, Australia
[g] Department of Neurology, Austin Health, Melbourne, Australia
[h] Department of Psychology and Neuroscience, Auckland University of Technology, Auckland, New Zealand

ARTICLE INFO

Keywords:
Temporal complexity
Multiscale entropy
Resting state network
Functional MRI
Human connectome project
Fluid intelligence
Reproducibility

ABSTRACT

It has been hypothesized that resting state networks (RSNs), extracted from resting state functional magnetic resonance imaging (rsfMRI), likely display unique temporal complexity fingerprints, quantified by their multiscale entropy patterns (McDonough and Nashiro, 2014). This is a hypothesis with a potential capacity for developing digital biomarkers of normal brain function, as well as pathological brain dysfunction. Nevertheless, a limitation of McDonough and Nashiro (2014) was that rsfMRI data from only 20 healthy individuals was used for the analysis. To validate this hypothesis in a larger cohort, we used rsfMRI datasets of 987 healthy young adults from the Human Connectome Project (HCP), aged 22-35, each with four 14.4-min rsfMRI recordings and parcellated into 379 brain regions. We quantified multiscale entropy of rsfMRI time series averaged at different cortical and subcortical regions. We performed effect-size analysis on the data in 8 RSNs. Given that the morphology of multiscale entropy is affected by the choice of its tolerance parameter (r) and embedding dimension (m), we repeated the analyses at multiple values of r and m including the values used in McDonough and Nashiro (2014). Our results reinforced high temporal complexity in the default mode and frontoparietal networks. Lowest temporal complexity was observed in the subcortical areas and limbic system. We investigated the effect of temporal resolution (determined by the repetition time T_R) after downsampling of rsfMRI time series at two rates. At a low temporal resolution, we observed increased entropy and variance across datasets. Test-retest analysis showed that findings were likely reproducible across individuals over four rsfMRI runs, especially when the tolerance parameter r is equal to 0.5. The results confirmed that the relationship between functional brain connectivity strengths and rsfMRI temporal complexity changes over time scales. Finally, a non-random correlation was observed between temporal complexity of RSNs and fluid intelligence suggesting that complex dynamics of the human brain is an important attribute of high-level brain function.

1. Introduction

The human brain is a *complex* hierarchy of modules that are dynamically interacting with each other at micro, meso and macro scales (Bassett and Bullmore, 2006; Park and Friston, 2013). Anatomically distinct, but functionally connected regions of the cortex that simultaneously fluctuate over time are referred to as *resting state networks* (*RSNs*). RSNs are intrinsic organizations of functional connectivity in the brain that are communicating with each other even in the absence of overt cognitive tasks (Beckmann et al., 2005; Biswal et al., 1995; Fox et al., 2005). These functional brain networks can be derived from resting state functional magnetic resonance imaging (rsfMRI), and are supporting a variety of sensory, cognitive and behavioural functions (van den Heuvel and Hulshoff Pol, 2010; Seeley et al., 2007). Perturbed

* Corresponding author at: Institute of Bioengineering, Center for Neuroprosthetics, Center for Biomedical Imaging, EPFL, Lausanne, Switzerland.
E-mail addresses: amir.omidvarnia@epfl.ch (A. Omidvarnia), azalesky@unimelb.edu.au (A. Zalesky), sina.mansour.lakouraj@gmail.com (S. Mansour L.), dimitri.vandeville@epfl.ch (D. Van De Ville), graeme.jackson@florey.edu.au (G.D. Jackson), mangor.pedersen@aut.ac.nz (M. Pedersen).

https://doi.org/10.1016/j.neuroimage.2021.117760
Received 13 October 2020; Received in revised form 18 December 2020; Accepted 5 January 2021
Available online 22 January 2021

functionality of RSNs contributes to a range of brain diseases including epilepsy (Gao et al., 2018), Alzheimer's disease (Brown et al., 2018), autism (Cherkassky et al., 2006), depression (Greicius et al., 2007) and schizophrenia (Ohta et al., 2018). Although alterations of RSNs have been subject to numerous studies, characterization of their *temporal complexity* remains an open question in the brain sciences (Bassett and Gazzaniga, 2011; Bassett et al., 2012; McDonough and Nashiro, 2014; Mišić et al., 2011; Pedersen et al., 2017; Sokunbi et al., 2014; Thompson et al., 2017; Wang et al., 2018a; 2018b). In the context of this study, temporal complexity is referred to as a balanced dynamical behaviour between pure regularity and complete irregularity in the time domain. This is a significant challenge in modern neuroscience because temporal complexity may provide a quantitative view of brain function at the phenomenological level which in turn, may lead to the development of more efficient diagnostic and prognostic markers of brain diseases.

Functional co-activations associated with RSNs fluctuate over time (Chang and Glover, 2010; Liu and Duyn, 2013). Until recently, most studies would treat functional brain connectivity as a *static* entity. The emergence of advanced neuroimaging techniques such as fast rsfMRI have opened up a new avenue for studying the dynamics of functional connectivity (Preti et al., 2017). There is now a consensus that this dynamical behaviour resides between temporal order and disorder (Goldberger et al., 1990; Goldberger, 1996; Lynn and Bassett, 2018). Temporal complexity of brain dynamics arises from interactions across numerous sub-components in the brain (McDonough and Nashiro, 2014) and can be affected by internal and/or external factors such as sensory inputs, attention and drowsiness (Shine et al., 2019). Conceptualization of this complexity includes but not limited to, self-similarity of EEG micro-state sequences (Britz et al., 2010; Van De Ville et al., 2010), dynamics of microscopic and mesoscopic neural networks in the brain (Bassett and Bullmore, 2006; Valverde et al., 2015) and neuronal oscillations associated with different brain regions (Hawrylycz et al., 2012).

Several attempts have been made to characterize the temporal complexity of RSNs using rsfMRI data including time-frequency analysis (Chang and Glover, 2010), independent components analysis (Allen et al., 2012), point process analysis (Tagliazucchi et al., 2012), sliding window analysis (Zalesky et al., 2014), phase synchrony analysis (Omidvarnia et al., 2016; Pedersen et al., 2018), auto-regressive modelling (Liégeois et al., 2019) and nonlinear analysis (McDonough and Nashiro, 2014; McIntosh et al., 2014; 2008; Pedersen et al., 2017) (see Preti et al., 2017 for a detailed review). An important form of temporal complexity in brain function can be observed through *multiscale entropy* analysis of RSN dynamics (McDonough and Nashiro, 2014). Multiscale entropy (Costa and Goldberger, 2015; Costa et al., 2002) quantifies the rate of generation of new information in a dynamical process by computing sample entropy (Richman and Moorman, 2000) over multiple temporal scales. Each scale provides a specific time resolution through coarse-graining of the input signals. For example, random signals such as white noise have high sample entropy values at fine scales (i.e., fast fluctuations) which drop gradually in value at large scales (i.e., slow fluctuations). On the other hand, complex signals such as random walk or biosignals generate a more consistent sample entropy curve over different time scales, due to repeating information-bearing patterns across multiple time resolutions (Costa and Goldberger, 2015; Costa et al., 2002; Maxim et al., 2005; Wang et al., 2018a).

In this paper, we investigated if the dynamics of RSNs can be differentiated based on their temporal complexity, quantified via multiscale entropy. To this end, we aimed to validate the existence of multiscale entropy fingerprints in rsfMRI-based RSNs. This hypothesis was tested in McDonough and Nashiro (2014) using rsfMRI datasets of 20 healthy subjects from the Human Connectome Project (HCP) (Van Essen et al., 2012) via multiscale entropy analysis in four RSNs: default mode, central executive, as well as the left and right frontoparietal networks (Fig. 1). Given the capacity of RSN complexity as an imaging-based marker of brain function in health and disease, we aimed to investigate this hypothesis in a larger sample cohort of 987 rsfMRI datasets from the HCP database. We included 8 RSNs in this study, with a particular focus on to what extent rsfMRI results are dependent on the tolerance parameter r, embedding dimension m and temporal resolution of rsfMRI in multiscale entropy analysis. We also conduced test-retest and effect-size analyses to delineate the reproducibility of RSN complexity across multiple rsfMRI scans and over subjects. We hypothesized that temporal complexity of brain function is related to higher order cognitive processes such as fluid intelligence or people's capacity to reason and think flexibly. Lastly, we looked into the potential link between functional brain connectivity and temporal complexity of RSNs at different time scales.

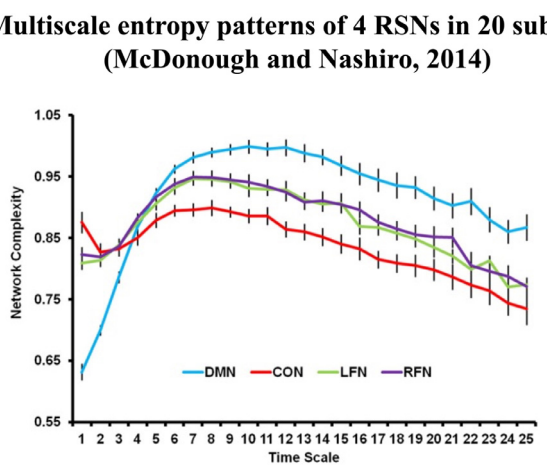

Fig. 1. Multiscale entropy patterns of 4 RSNs (default mode network or DMN, central executive network or CON, left frontoparietal network or LFN, right frontoparietal network or RFN) in 20 subjects reported in McDonough and Nashiro (2014). The image, taken from McDonough and Nashiro (2014), is published under theterms of Creative Commons Attribution Licence (CC BY), allowing for reproduction.

2. Materials and methods

2.1. RsfMRI data, parcellation masks and preprocessing

We used a subset of the HCP database (Van Essen et al., 2012) including 987 rsfMRI datasets (N_{subj}=987). Each subject participated in two separate rsfMRI sessions on two different days, with two acquisitions per day, i.e., left to right and right to left slicings. We refer to these recordings as four fMRI runs throughout this paper. Each run was of length 14.4 minutes (or 1200 time points) with a voxel size of $2\times2\times2$ millimeters and the repetition time (T_R) of 720 ms in a 3T scanner. The following preprocessing steps were applied on each dataset: 1) echo planar imaging gradient distortion correction, 2) motion correction, 3) field bias correction, 4) spatial transformation, 5) normalization into a common Montreal Neurological Institute space (Glasser et al., 2013) and 6) artefact removal using ICA-FIX (Salimi-Khorshidi et al., 2014). A parcellation mask (Glasser et al., 2013) was used to parcellate the gey matter into 360 cortical and 19 subcortical regions of interest (N_{ROI}=379). The preprocessed datasets are publicly available at the HCP website under an Open Access Data plan agreement.

2.2. Multiscale entropy analysis

While there are several definitions of signal entropy in the literature, our focus here is on multiscale entropy analysis (Costa and Goldberger, 2015; Costa et al., 2002). This technique is an extended version of *sample entropy* (Richman and Moorman, 2000) over multiple time scales.

2.2.1. Sample entropy

Sample entropy is a signal complexity measure which treats each short piece of an input signal $\mathbf{x}$ as a *template* to search for any *neighbouring* templates throughout the entire length of the signal. A template $\mathbf{X}_i^m$ is defined as[1]:

$$\mathbf{X}_i^m = \{x_i,\ x_{i+1}, ..., x_{i+m-1}\}, i = 1, ..., N - m + 1. \tag{1}$$

where N is the number of time points in $\mathbf{x}$ and m is the *embedding dimension* parameter. Two templates $\mathbf{X}_i^m$ and $\mathbf{X}_j^m$ are considered as neighbours if their *Chebyshev* distance $d(\mathbf{X}_i^m, \mathbf{X}_j^m)$ is less than a *tolerance* parameter r. It leads to an r-neighbourhood conditional probability function $C_i^m(r)$ for any vector $\mathbf{X}_i^m$ in the m-dimensional reconstructed phase space:

$$C_i^m(r) = \frac{1}{N - m + 1} B_i^m(r),\ i = 1, ..., N - m + 1, \tag{2}$$

where $B_i^m(r)$ is given by:

$$B_i^m(r) = \sum_{j=1}^{N-m} \Psi(r - d(\mathbf{X}_i^m, \mathbf{X}_j^m)), \tag{3}$$

where $\Psi(.)$ is the Heaviside function, defined as:

$$\Psi(a) = \begin{cases} 0 & a < 0 \\ 1 & a \geq 0. \end{cases} \tag{4}$$

The Chebyshev distance d is defined as:

$$d(\mathbf{X}_i^m, \mathbf{X}_j^m) := \max_k(|x_{i+k} - x_{j+k}|,\ k = 0, ..., m - 1). \tag{5}$$

Sample entropy is then given by:

$$SampEn(\mathbf{x}, m, r) = \lim_{N\to\infty} ln\ \frac{\mathcal{B}_m^r}{\mathcal{B}_{m+1}^r}, \tag{6}$$

where $\mathcal{B}_m^r$ is the average of $B_i^m(r)$ over all templates:

$$\mathcal{B}_m^r = \frac{1}{N - m} \sum_{i=1}^{N-m} B_i^m(r). \tag{7}$$

Since $d(\mathbf{X}_i^m, \mathbf{X}_j^m)$ is always smaller than or equal to $d(\mathbf{X}_i^{m+1}, \mathbf{X}_j^{m+1})$, $\mathcal{B}_{m+1}^r$ will always take smaller or equal values than $\mathcal{B}_m^r$. Therefore, sample entropy is always non-negative. The tolerance parameter r plays a central role in any sample entropy analysis, because it defines the probability of neighbourhood (i.e., similarity) between two templates in the reconstructed phase space. It is important to multiply r by the standard deviation of $\mathbf{x}$ to account for amplitude variations across different signals (Richman and Moorman, 2000). In this study, we used the embedding dimension of m=2 and the tolerance parameter of r=0.5 for sample entropy analysis, as adapted in McDonough and Nashiro (2014). In addition, we used the tolerance parameter of r=0.15, a widely used option in the literature (see Niu et al., 2018; Yang et al., 2011 as examples), as well as a range of embedding dimensions from m=3 to m=10.

2.2.2. Multiscale entropy

Multiscale entropy extracts sample entropy after *coarse-graining* of the input signal $\mathbf{x}$ at a range of time scales τ (Costa et al., 2002). A coarse-grained vector $\mathbf{x}^\tau = \{x_i^\tau\}$ is defined as:

$$x_i^\tau = \frac{1}{\tau} \sum_{k=(i-1)\tau+1}^{i\tau} x_k, \quad \tau = 1, 2, ..., \tau_{max}, \quad i = 1, ..., [N/\tau], \tag{8}$$

where $\mathbf{x}^1 = \mathbf{x}$. Following (McDonough and Nashiro, 2014), we set τ_{max} to 25. At the group level, we averaged the multiscale entropy curves over subjects and calculated the standard deviation at each scale.

2.2.3. Complexity index

To reduce the dimensionality of multiscale entropy patterns to a single value, a complexity index is defined for the i^{th} RSN as the area under each multiscale entropy curve over all scales, divided by the maximum number of scales (i.e., τ_{max}) (Weng et al., 2015):

$$M_i = \frac{1}{\tau_{max}} \int_1^{\tau_{max}} SampEn(\mathbf{x}_i^\tau, m, r)\ d\tau. \tag{9}$$

2.2.4. The role of rsfMRI temporal resolution

Given the relatively short repetition time of rsfMRI time series in the HCP database (T_R=0.72 s), we investigated to what extent the observed complex dynamics of RSNs is sensitive to rsfMRI temporal resolution. This is an important issue to check, because T_R values longer than 1 s are common across research and clinical centres. We resembled longer T_R's in our datasets by downsampling of the rsfMRI time series in the HCP database. To this end, we calculated the complexity indices of RSNs after downsampling of the rsfMRI time series at the rates of 2 and 4, resembling the repetition times of T_R=1.44 s and T_R=2.88 s, respectively.

2.2.5. Effect size analysis using the Hedges' g measure

We quantified the difference between complex dynamics of RSNs by pair-wise effect size analysis of the complexity index distributions at three temporal resolutions (i.e., original T_R of 0.72 s and two downsampling rates) as well as multiple combinations of the multiscale entropy parameters (i.e., r=0.15, 0.5 and m=2 to 10). To this end, we used the Hedges' $g_{i,j}$ statistic, defined as (Hedges, 1981):

$$g_{i,j} = \frac{M_i - M_j}{\sigma_{i,j}}, \tag{10}$$

where M_i and M_j are the group mean complexity indices of the i^{th} and j^{th} RSNs, respectively, and $\sigma_{i,j}$ is the squared mean of the associated standard deviations computed as:

$$\sigma_{i,j} = \sqrt{\frac{\sigma_i^2 + \sigma_j^2}{2}}. \tag{11}$$

The confidence interval and p-value of the Hedges' g measures were calculated through bootstrapping (2000 random samplings of the original time series with replacement)[2].

2.2.6. Test-retest analysis using the intra-class correlation coefficient

In order to investigate the reproducibility of multiscale entropy patterns extracted from RSNs at different temporal resolutions, we computed *intra-class correlation* coefficient of sample entropy values at single time scales and over four rsfMRI scans (N_{run}=4). Following (Hodkinson et al., 2013), we chose the third intra-class correlation coefficient measure defined in Shrout and Fleiss (1979) for test-retest analysis as:

$$ICC_i(\tau) = \frac{BMS_i(\tau) - EMS_i(\tau)}{BMS_i(\tau) + (N_{run} - 1)EMS_i(\tau)}, \tag{12}$$

where $BMS_i(\tau)$ and $EMS_i(\tau)$ are the *between-subjects mean square* and the *error mean square* of sample entropy values, respectively, for the i^{th} RSN at the time scale τ. We considered the intra-class correlation coefficient values below 0.4 as poor reliability, between 0.4 and 0.6 as fair reliability and between 0.6 and 0.8 as good reliability (Hodkinson et al., 2013).

2.3. Temporal complexity of RSNs and cognition

We also tested whether temporal complexity of rsfMRI is related to higher order cognition. For each subject (N_{subj} = 987), we selected five well-validated domain-specific behavioural variables

[1] In all equations, scalar variables are in normal font, while vector variables are in bold.

[2] The effect size analysis toolbox associated with Hentschke and Stüttgen (2011) is available at the MATLAB File Exchange website.

($N_{beh} = 5$) involved in higher order cognition; *i*) the Eriksen flanker task (*Flanker_Unadj* - measuring response inhibition and task switching); *ii*) the Wisconsin Card Sorting Test (*CardSort_Unadj* - measuring cognitive flexibility); *iii*) the N-back task (*WM_Task_acc* - measuring working memory performance); *iv*) the Ravens task (*PMAT24_A_CR* - measuring fluid intelligence); and *v*) the relational task (*Relational_Task_Acc* - measuring planning and reasoning abilities). See Barch et al. (2013), for full information about behavioural variables included in the HCP. We defined a multiple linear regression model with N_{beh} independent variables as follows:

$$\hat{\mathbf{M}}_i = \hat{\beta}_i(0)\mathbf{1} + \hat{\beta}_i(1)\mathbf{b}_1 + ... + \hat{\beta}_i(N_{beh})\mathbf{b}_{N_{beh}}, \quad (13)$$

where $\mathbf{1}$ is a column vector of 1's, $\hat{\mathbf{M}}_i \in \mathbb{R}^{N_{subj}\times 1}$ is the predicted vector of subject-specific complexity indices in the i^{th} RSN and $\mathbf{b}_k \in \mathbb{R}^{N_{subj}\times 1}$ is the associated vector of the k^{th} behavioural measure ($k = 1, ..., N_{beh}$). For each estimated coefficient $\hat{\beta}_i(k)$, we performed a *t*-test at the significance level of 0.05 whether the coefficient is equal to zero or not. To assess whether the correlation coefficients between real complexity indices $\mathbf{M}_i$ and their predicted associates $\hat{\mathbf{M}}_i$ are statistically significant, we performed a permutation testing for each RSN where we permuted the order of subjects in $\mathbf{M}_i$, refitted the model and repeated this procedure for 10000 times. It led to an empirical null distribution for each network.

To assess the contribution of each behavioural variable into the temporal complexity of RSNs, we performed a bidirectional step-wise regression analysis where the independent variables were added or removed based on their importance to the fitted model in an iterative fashion at the significance level of 0.05 (Draper and Smith, 1967). The procedure continues until no further improvement can be obtained in the goodness of fit of the regression model.

3. Results

3.1. Simulation: multiscale entropy analysis of colored noise

To demonstrate the capacity of multiscale entropy analysis for encoding signal dynamics, we simulated 100 realizations of four colored noise signals (white, blue, pink and red) with 1200 time-points and computed their multiscale entropy patterns (m=2, r=0.15). See Fig. 2-A, B for exemplary realizations of the noise types and their associated power spectral densities. As Fig. 2-C shows, multiscale entropy curves of each noise type are distinct and can be considered as their dynamical signature. The associated complexity index values are also an informative indicator of the time-varying nature in each noise type, except for white and red noise whose complexity distributions fully overlap (Fig. 2-D). Among the four, blue and white noises lead to lower complexity indices, while pink and red noises resemble complex signals due to their $1/f^{\beta}$ spectral density functions and fractal properties (Costa et al., 2005).

3.2. RSNs are temporally complex

We observed distinct multiscale entropy patterns between cortical and subcortical parts of RSNs (379 regions in total illustrated as blue and red curves in the middle rows of Figs. 3 and 4). A visual comparison between cortical/subcortical multiscale entropy curves and simulated noise processes (Fig. 2-C) suggests that the entropy patterns of higher-order RSNs are closer to the morphology of synthetic complex signals such as pink noise and red noise, while subcortical regions and limbic network are more similar to non-complex signals such as white noise and blue noise. This observation was more evident for the tolerance parameter r=0.5 compared to r=0.15 (top row of Fig. 3 in contrast to the top row of Fig. 4). Our multiscale entropy analysis of RSNs at r=0.5, m=2 and τ=1 to 25 was in line with the findings of McDonough and Nashiro (2014) where the default mode and frontoparietal networks were studied. Possible differences between (McDonough and Nashiro, 2014) and our study may be due to the fact that we used a different brain parcellation and spatial definition of RSNs compared to (McDonough, Nashiro, 2014). As the third rows of Figs. 3 and 4 illustrate, multiscale entropy patterns of RSNs preserve a consistent order of complexity index across 8 RSNs with the frontoparietal (FP) network and default mode network (DMN) as the most complex and the subcortical (SUBC) and limbic (L) networks as the least complex RSNs. Visual (VIS) and somatomotor (SM) and ventral attention (VA) networks also sit in between. This ordering remains relatively consistent after changing of the multiscale entropy parameters, despite differences in the morphology of RSN entropy patterns. The tolerance parameter r=0.5 leads to a more stable morphology over different embedding dimensions m, while the entropy curves associated with r=0.15 represent considerable amount of undefined values for dimensions $m \geq 4$ and therefore, less discrimination between the temporal complexity of RSNs (bottom row in Fig. 4). The undefined values of multiscale entropy are caused by the zero values of B_m^r in Eq. (6) due to the lack of neighbouring templates $\mathbf{X}_i^m$ and $\mathbf{X}_j^m$ at the tolerance parameter r. The effect size analysis of the pair-wise comparisons across RSNs are illustrated in Fig. 6 and summarized in the first columns of Table S6 (for r=0.5 and m=2) and Table S7 (for r=0.15 and m=2). According to the tables, RSNs are highly distinguishable based on their associated complexity indices at both values of r (Hedges' g of 2.33±1.68 for r=0.5 and 2.55±1.72 for r=0.15).

3.3. Head motion is temporally less complex than RSN dynamics

A striking observation in the top rows of Figs. 3 and 4 is the distinctive multiscale entropy pattern of head motion, quantified by frame-wise displacement of each subject during the rsfMRI runs, in contrast to the dynamics of RSNs. Frame-wise displacement of an rsfMRI recording is defined as the sum of the absolute values of the derivatives of its associated six realignment parameters (Power et al., 2014). As the figures suggest, head motion has a considerably lower temporal complexity than rsfMRI time series which makes it comparable with the dynamics of white and blue noises in Fig. 2. This distinction is most obvious across the lower time scales ($\tau \leq 10$). Notably, an increase in the embedding dimension m has a detrimental impact on the multiscale entropy patterns of head motion at r=0.15 and increases the standard deviation at each time scale drastically (see Fig. 4). In fact, embedding dimensions above 3 lead to very poor outcome at r=0.15. From this perspective, the choice of r=0.5 is more appropriate for multiscale entropy analysis of rsfMRI and head motion, as it is more robust to the changes of embedding dimension.

3.4. Temporal complexity of RSNs is stronger at shorter T_R's

Fig. 5 and Figs. S1 to S3 illustrate multiscale entropy curves of 8 RSNs using the tolerance parameters r=0.5, 0.15 and embedding dimensions m=2,3,4, at the downsampling rates of 2 (equivalent with a T_R of 1.44 s) and 4 (equivalent with a T_R of 2.88 s). We observed that the morphology of entropy values was clearly influenced by the temporal resolution of the underlying data (see Fig. 5 and Fig. S2 versus Fig. 3 for r=0.5 and Figs. S1 and S3 versus Fig. 4 for r=0.15). This change was reflected as a decrease in the mean values of the complexity indices across RSNs (see the bottom rows in all figures). Having said that, pair-wise discrimination between the complexity index distributions of RSNs was still preserved after downsampling (see the second and third columns of Tables S6 and S7). However, a consistent reduction was introduced to the pair-wise Hedges' g statistics of effect size analysis in longer T_R's (from 2.33±1.68 to 1.83±1.33 and 1.17±0.79 for r=0.5 and from 2.55±1.72 to 2.06±1.32 and 0.33±0.22 for r=0.15). Fig. 6 illustrates the color-coded Hedges' g measures of rsfMRI complexity index distributions using two tolerance parameter values at three temporal resolutions and using the embedding dimension of m=2.

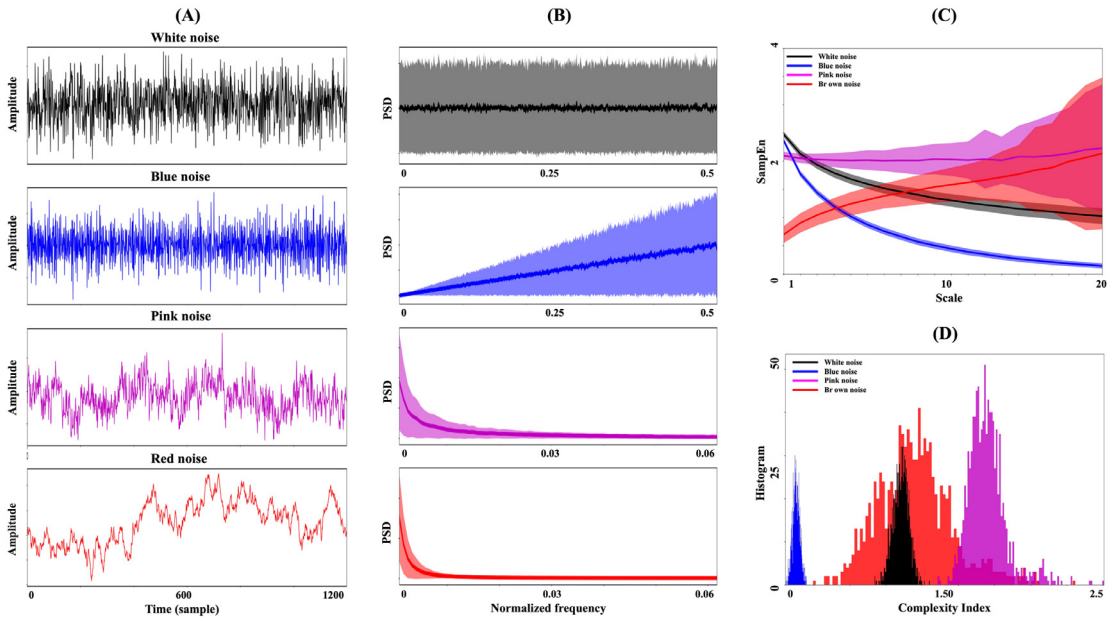

Fig. 2. Multiscale entropy of white noise in black color, blue noise in blue color, pink noise in pink color and red (Brown) noise in red color (m=2, r=0.15). For each noise type, 100 random realizations were generated. Column (A) Exemplary realizations in the time domain. Column (B) Shaded error bars of power spectral density functions associated with 100 realizations. (C) Distributions of multiscale entropy patterns over 100 realizations. Shaded regions show one standard deviation from the mean curve. (D) Distributions of complexity index values.

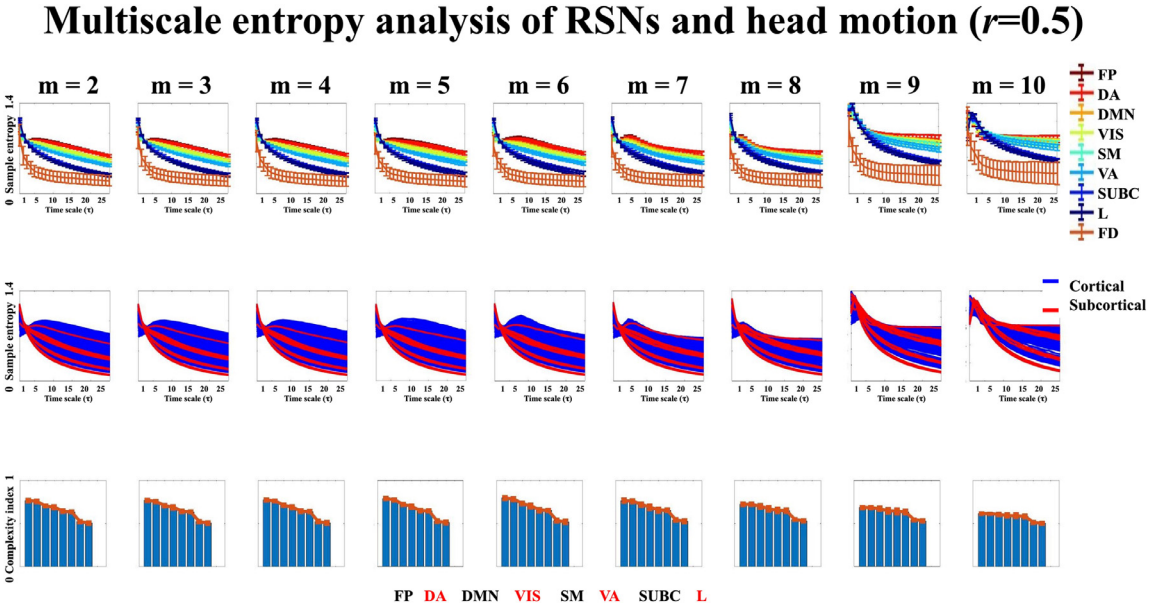

Fig. 3. **Top row**: Multiscale entropy patterns of 8 RSNs as well as head motion (frame-wise displacement), averaged over 987 subjects and four rsfMRI runs, with the tolerance parameter r=**0.5** and a range of embedding dimensions m from 2 to 10. In all plots, each curve represents the average and the error bars demonstrate one standard deviation over subjects. The entropy curves have been color-coded according to their complexity indices. The multiscale entropy curve of head motion (labeled as *FD*) has a distinct pattern compared to RSNs. **Middle row**: ROI-wise multiscale entropy patterns, averaged over 987 subjects and four rsfMRI runs for the same parameter sets as the first row. The entropy patterns associated with the cortical regions (N_{ROI}=360) are in blue color and associated with the subcortica regions (N_{ROI}=19) are in red color. The brain parcels were obtained according to Glasser et al. (2013). **Bottom row**: Bar plots of the group-mean complexity indices associated with the RSN-wise multiscale entropy patterns in the first row. The RSNs have been sorted according to their group-mean complexity indices. In all plots, the bars are labeled as follows: FP, DA, DMN, VIS, SM, VA, SUBC, L. **Abbreviation**: FP = Frontoparietal, DA = Dorsal Attention, DMN = Default mode network, VIS = Visual, SM = Somatomotor, VA = Ventral Attention, SUBC = Subcortical, L = Limbic, FD = Frame-wise Displacement (extracted from head motion parameters). See Yeo et al. (2011) for the illustrations of RSNs.

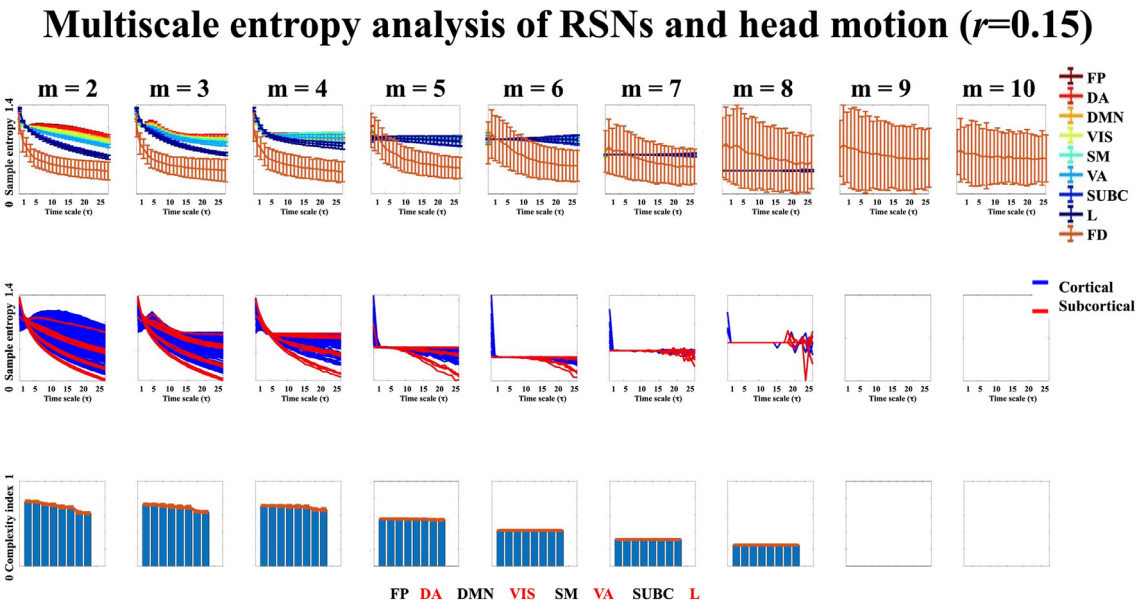

Fig. 4. Top row: Multiscale entropy patterns of 8 RSNs as well as head motion (frame-wise displacement), averaged over 987 subjects and four rsfMRI runs, with the tolerance parameter r**=0.15** and a range of embedding dimensions m from 2 to 10. In all plots, each curve represents the average and the error bars demonstrate one standard deviation over subjects. The entropy curves have been color-coded according to their complexity indices. The multiscale entropy curve of head motion (labeled as *FD*) has a distinct pattern compared to RSNs. **Middle row**: ROI-wise multiscale entropy patterns, averaged over 987 subjects and four rsfMRI runs for the same parameter sets as the first row. The entropy patterns associated with the cortical regions (N_{ROI}=360) are in blue color and associated with the subcortical regions (N_{ROI}=19) are in red color. The brain parcels were obtained according to Glasser et al. (2013). **Bottom row**: Bar plots of the group-mean complexity indices associated with the RSN-wise multiscale entropy patterns in the first row. The RSNs have been sorted according to their group-mean complexity indices. Blanc panels represent undefined entropy values. In all plots, the bars are labeled as follows: FP, DA, DMN, VIS, SM, VA, SUBC, L. **Abbreviation**: FP = Frontoparietal, DA = Dorsal Attention, DMN = Default mode network, VIS = Visual, SM = Somatomotor, VA = Ventral Attention, SUBC = Subcortical, L = Limbic, FD = Frame-wise Displacement (extracted from head motion parameters). See Yeo et al. (2011) for the illustrations of RSNs.

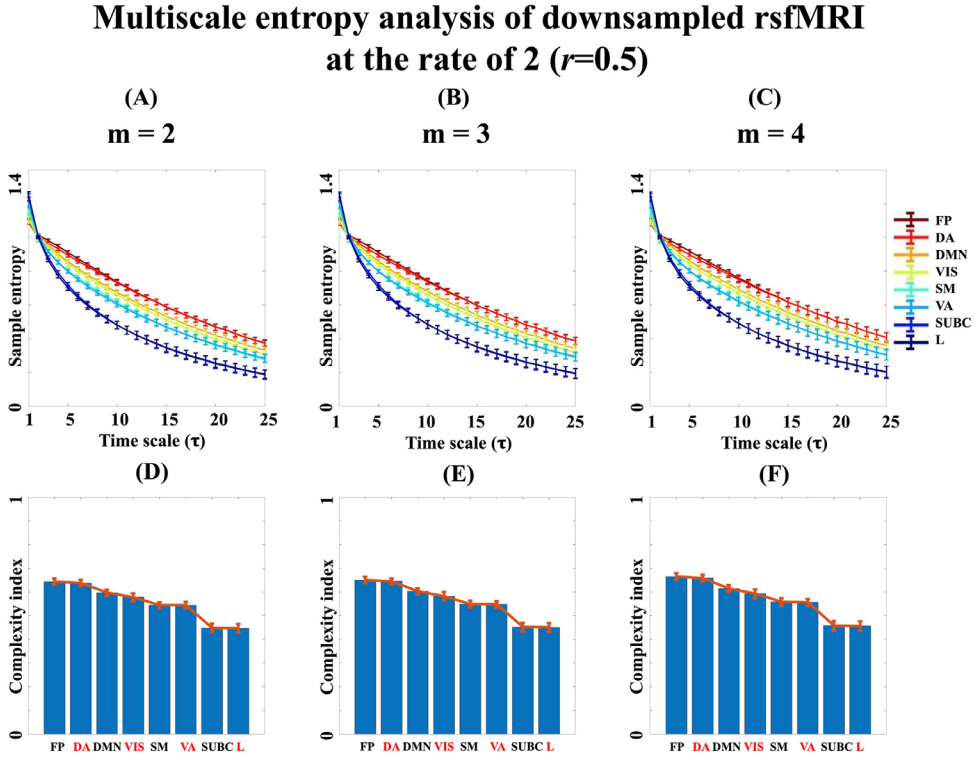

Fig. 5. The effect of downsampling on the multiscale entropy curves of HCP, averaged over 987 subjects and four rsfMRI runs. (A)-(C): Error bars of multiscale entropy curves after downsampling of rsfMRI time series **at the rate of 2 for the embedding dimensions** m=2,3,4 and the tolerance parameter r**=0.5**. The entropy curves have been color-coded according to their complexity indices (normalized area under their curve). (D)-(F): Mean plots of the complexity index values extracted from the multiscale entropy curves of (A)-(C), respectively. **Abbreviation**: FP = Frontoparietal, DA = Dorsal Attention, DMN = Default mode network, VIS = Visual, SM = Somatomotor, VA = Ventral Attention, SUBC = Subcortical, L = Limbic. See Yeo et al. (2011) for the illustrations of RSNs.

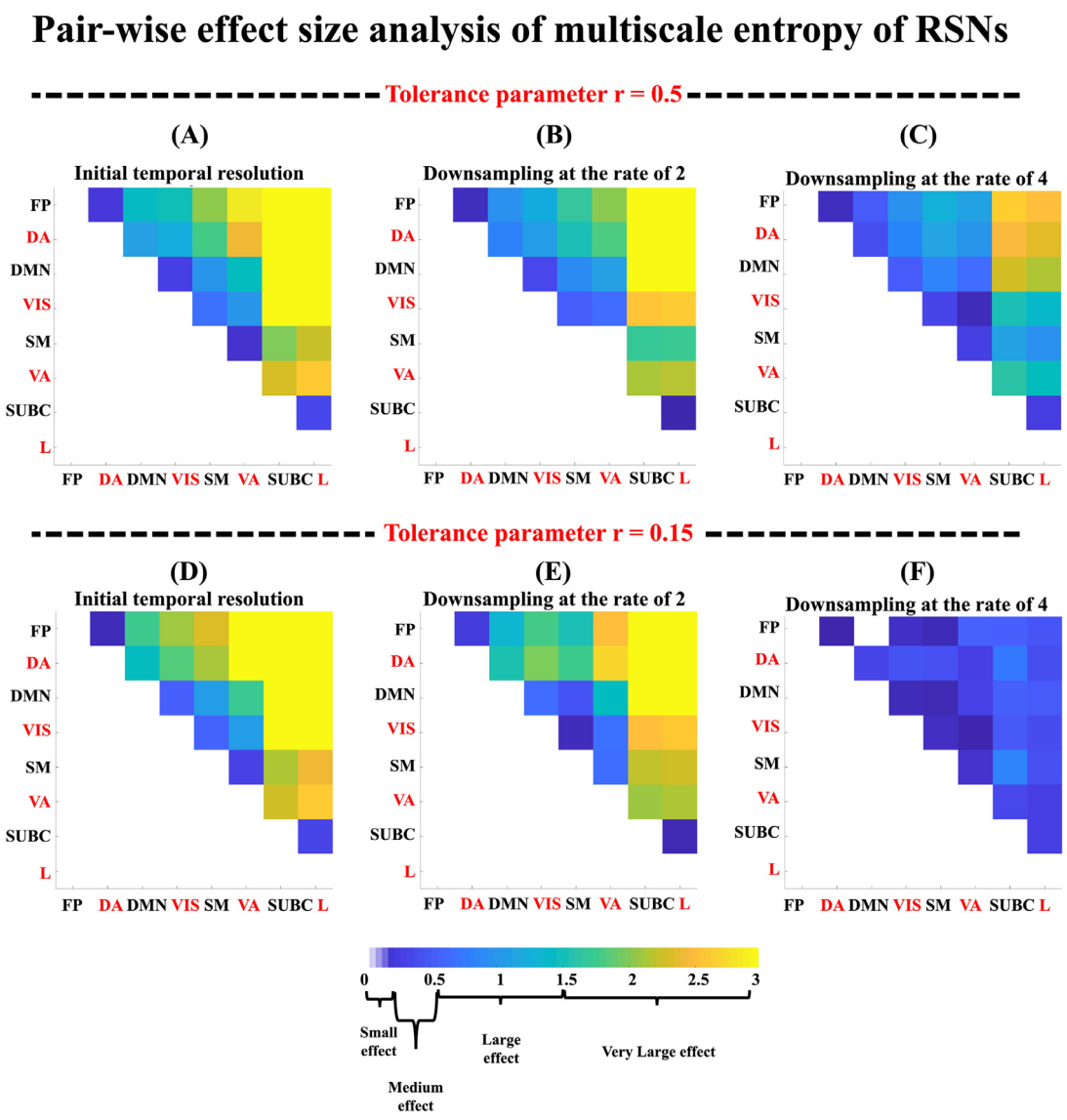

Fig. 6. Hedges' g statistics obtained from effect size analysis of the complexity index distributions calculated for all pairs of RSNs. The analysis has been repeated for the embedding dimension m=2, the tolerance parameters (r=0.15,0.5) and at three downsampling scenarios (no downsampling, downsampling at the rate of 2 and downsampling at the rate of 4). The Hedges' g values of less than 0.2 imply small effect, 0.2 to 0.5 are considered as medium effect, 0.5 to 1.5 are deemed as large effect and above 1.5 represent very large effect. **Abbreviation**: FP = Frontoparietal, DA = Dorsal Attention, DMN = Default mode network, VIS = Visual, SM = Somatomotor, VA = Ventral Attention, SUBC = Subcortical, L = Limbic. See Yeo et al. (2011) for the illustrations of RSNs.

3.5. Temporal complexity of RSNs is reproducible

We performed a test-retest analysis to assess whether complexity of RSNs is reproducible across different rsfMRI runs of HCP. We computed multiscale entropy curves of 987 datasets for four rsfMRI runs of length 14.4 minutes separately (i.e., 4×1200 T_R's). We computed the intra-class correlation coefficient of scale-dependent sample entropy values over all subjects and four sessions for 8 RSNs (Yeo et al., 2011) and 25 time scales. We repeated the test-retest analysis for two tolerance parameters r=0.15, 0.5, three embedding dimensions m=2,3,4 and three rsfMRI temporal resolutions. The results are presented as color-coded maps in Fig. S5. As this figure shows, the tolerance parameter r=0.5 and m=2 at the original temporal resolution of rsfMRI (T_R=720 ms) yielded the greatest intra-class correlation coefficient scores. At all temporal resolutions, reproducibility decreased from r=0.5 to r=0.15. Also, an increase in the embedding dimension m had a detrimental impact on the reproducibility of RSN complexity indices at r=0.15, while the values associated with r=0.5 were almost unchanged. Given that intra-class correlation coefficient decreases as a function of greater downsampling, it is possible that longer T_R's in the rsfMRI recordings have a negative effect on the reproducibility of RSN complexity. Amongst the 8 RSNs, the default mode and frontoparietal networks had strongest test-retest reliability. Lowest reproducibility was seen in the subcortical network.

3.6. Temporal complexity of RSNs correlates with higher order cognition

A permutation test with 10000 shufflings over subjects showed that correlation coefficients associated with all RSNs were above the 95th percentile of the empirical null distributions (Fig. S4). This means that the correlation between original and predicted rsfMRI complexity was statistically higher than expected by chance. We performed step-wise regression analysis between five behavioural variables and complexity indices of 8 RSNs for m=2, r = 0.15, 0.5 as well as no downsampling, downsampling at the rate of 2 and downsampling at the rate of 4 (6 dif-

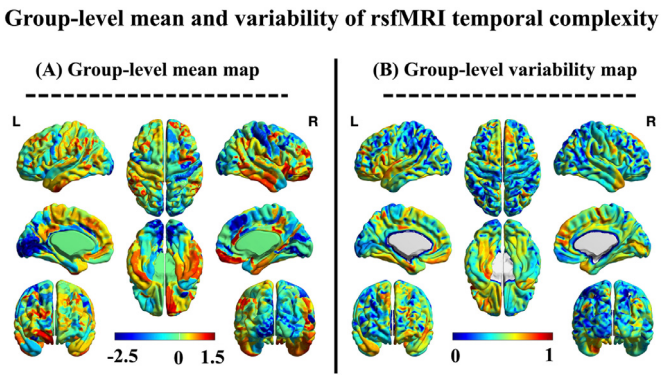

Fig. 7. (A) Grand-mean brain map of RSN complexity indices, (B) normalized standard deviation map of RSN complexity indices. Both maps were extracted from rsfMRI datasets of 987 HCP subjects, averaged over four resting state runs. Each dataset was parcellated using the Glasser atlas with 379 regions (Glasser et al., 2016). The complexity index is defined as the area under the curve of multiscale entropy. The complexity indices were z-scored to aid visualization.

ferent conditions in total). The results have been summarized in Tables S8 to S13. As the tables show, fluid intelligence was the only winning variable in all RSNs under different scenarios. Amongst the five cognitive measures, fluid intelligence (Variable 4) displayed statistically significant (positive) regression coefficients (β's) with 8 RSNs at all temporal resolutions for both tolerance parameters r=0.5 and r=0.15. We corrected each set of 8 RSN-specific p-values and 5 behavioural variables (i.e., 40 tests, in total) using the false discovery rate method at the significance level of q-value no more than 0.05. It ensures that the likelihood of false-positive results across significant regression variables stays below 5% after multiple comparisons. In other words, the association between fluid intelligence and temporal complexity of RSNs is relatively robust against the choice of tolerance parameter r and downsampling of the rsfMRI time series.

3.7. Spatial distribution of rsfMRI complexity

Fig. 7 demonstrates the spatial distribution of complexity indices across 379 brain regions according to the brain parcellation of Glasser et al. (2013). The highest complexity indices in the brain map of Fig. 7-A are associated with FP, DMN and DA networks and the lowest values correspond to subcortical areas and the limbic system. More precisely, top five brain regions with the highest complexity values belong to left and right inferior parietal cortex (PGs, left and right PFm and left PF). Also, bottom five brain regions with the lowest complexity include left entorhinal cortex (EC), left and right nucleus accumbens as well as left and right pallidum. On the other hand, the lowest variability in Fig. 7-B was observed across regions with the highest mean complexity including left and right inferior parietal cortex (PFm and left PGs) as well as superior parietal cortex areas associated with DMN (IP1). In contrast, the highest variability was associated with left inferior temporal sulcus (TE2a), left ventro-medial visual areas (VMV1), left middle temporal gyrus (TE1m), Right insular granular complex (Ig) and right lateral temporal cortex (TF). See Glasser et al. (2016) for more information about specific functions of these brain areas. This finding is consistent with our RSN specific analysis that signal complexity is highest in frontoparietal networks and DMN. Table S1 summarizes the brain regions with highest/lowest mean complexity and variability of complexity at the group level.

We also investigated the relationship between functional brain connectivity and multiscale entropy of RSNs over time scales (McDonough and Nashiro, 2014). To this end, we extracted the *functional brain connectivity strengths* of 379 brain parcels over four rsfMRI runs leading to four brain maps for each subject. The functional connectivity strength of each ROI was defined as the sum of weights of *links* connected to that ROI. The links between ROIs were defined as the pair-wise correlation between their associated rsfMRI time series. We examined the spatial correlation between the average-run maps of sample entropy (i.e., scale-dependent multiscale entropy) and functional connectivity strengths for each RSN separately. As Fig. 8 illustrates, there is a negative correlation between functional connectivity and temporal complexity of RSNs at fine scales (i.e., between τ=3 for subcortical and limbic networks to τ=5 for frontoparietal, default mode and dorsal attention networks), while it turns to a positive correlation at coarse scales ($\tau \geq 6$). This observation is in line with the finding reported in McDonough and Nashiro (2014).

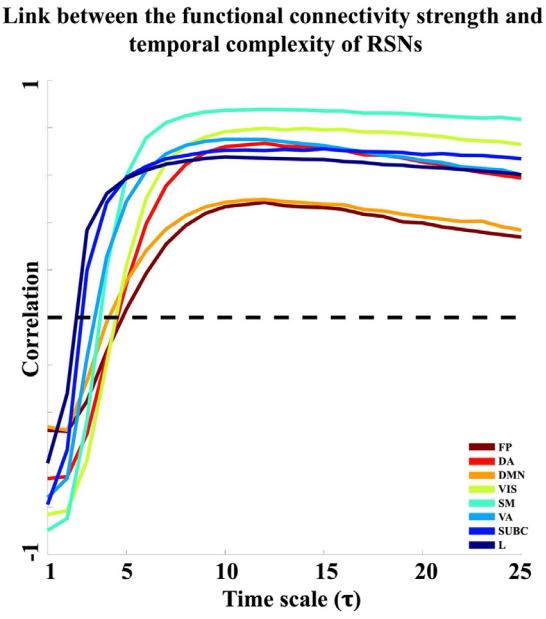

Fig. 8. The relationship between functional connectivity strength and temporal complexity of brain regions across different RSNs. The results have been averaged over 987 subjects and four rsfMRI runs. The networks have been color-coded according to their temporal complexity. The x-axis shows the time scales associated with the multiscale entropy patterns of RSNs. The y-axis represents the spatial correlation between the ROI-wise functional connectivity strengths and their corresponding temporal complexity indices across different networks.

4. Discussion

Our study validates the hypothesis of distinct multiscale entropy signatures in functional brain networks and reinforces the previous findings by McDonough and Nashiro (2014). We also build on previous research in several ways by: (*i*) increasing the number of subjects from 20 to 987, enabling a statistically more robust characterization of RSN complexity in the time domain, (*ii*) delineating temporal complexity in an additional four RSNs, (*iii*) comparing two values of the tolerance parameter r and multiple values of the embedding dimension m for multiscale entropy analysis, (*iv*) investigating the relationship between the temporal complexity of head motion and dynamics of RSNs, (*v*) investigating the effect of temporal resolution on the complexity of RSNs, (*vi*) analyzing the reproducibility of complex dynamics in functional networks over multiple recording sessions, and (*vii*) showing that signal complexity is related to higher-order cognitive processing.

The conceptual definition of temporal complexity may vary depending on context and data. In the context of our study, we refer to temporal complexity as a grey boundary between order and disorder over time. From this perspective, random fluctuations such as white noise have low temporal complexity, because they are completely disordered. Note that temporal complexity is not necessarily equivalent with high

unpredictability or high randomness. On the other hand, highly ordered signals such as a pure sine wave also have low complexity. RsfMRI sits in between these two exemplars because it represents spreading patterns of structured activity across multiple frequency components and temporal scales that are embedded in a random background (Hutchison et al., 2013; Preti et al., 2017; Richiardi et al., 2013; 2011). This complex behaviour arises from functional interactions of numerous subcomponents in the brain representing a balanced tuning between order and disorder (Bassett and Gazzaniga, 2011). Several internal and external factors such as sensory inputs, attention, drowsiness and imagination may also push brain dynamics towards either order or disorder, but stably (Shine et al., 2019). It remains an open question of how to quantify balanced fluctuations (Kirst et al., 2016) in brain function and delineate their relationship with human behaviour and cognition.

The dynamics of RSNs represent a continuum of multiscale entropy characteristics, from low complex regions across the entorhinal cortex (Fischl et al., 2009) and subcortical areas to brain regions resembling complex noise types (i.e., pink and red noise) within frontoparietal and default mode networks (Caspers et al., 2008). See Fig. 2-C in contrast to the first and second rows of Fig. 3 and Fig. 4. Our results suggest that the temporal complexity of RSNs is a highly discriminative feature that cannot be explained by head movement. Head motion, as quantified by frame-wise displacement, represents a considerably lower temporal complexity than the RSN dynamics. This difference is reflected in the multiscale entropy patterns of these signals and is significantly affected by the choice of the tolerance parameter r and the embedding dimension m. According to the results of this study, a tolerance parameter of $r = 0.5$ and an embedding dimension within the range of 2 to 5 lead to an acceptable separation between RSN dynamics and head motion as well as discrimination over RSNs. Large embedding dimensions in the multiscale entropy analysis can increase the distance quantity $d(\mathbf{X}_i^m, \mathbf{X}_j^m)$ and therefore, the probability of zero outputs occurring in the Heaviside step function in Eq. (3). This is specially the case when small tolerance values are used for the multiscale entropy analysis. Examples include the high occurrence of undefined entropy values for the combination of $r = 0.15$ and $m \geq 5$ in the second and third rows of Fig. 4. As presented in Tables S8 to S13, fluid intelligence seems to have the strongest linear relationship with the temporal complexity of rsfMRI compared to the other four behavioral measures. This measure refers to people's ability to provide logical solutions to specific problems, in novel situations where acquired knowledge cannot be retrieved (Cattell, 1963).

Vigilance is another important aspect of cognition whose influence on RSNs has been studied before (Laufs et al., 2012; Shen et al., 2016; Wong et al., 2013). It has been hypothesized that the temporal behaviour of RSNs is influenced by variations in vigilance (Laufs et al., 2012). Maintaining a constant level of wakefulness is difficult during resting state experiments, although HCP subjects are instructed to keep awake and visually fixate on a cross on a screen. However, it is still important to consider the potential impact of vigilance fluctuations on the multiscale entropy patterns of RSNs and their associated complexly indices. This can also influence the interpretation of which functional brain networks have more reliable brain complexity dynamics. The relationship between vigilance and temporal complexity of RSNs is regarded to future work.

Multiscale entropy patterns provide a more comprehensive picture about brain complexity than sample entropy at single time scales. In fact, single-scale sample entropy analysis could lead to misleading interpretations about the complexity of brain regions and functional networks. As demonstrated in the top rows of Figs. 3 and 4, the entropy values associated with different RSNs may get reverse over large scales (for example, before and after τ=3 at the tolerance parameter r=0.5 and the embedding dimension m=2). The distinction in complexity between cortex and subcortex could be partly related to lower temporal signal to noise ratio in rsfMRI time series within subcortical nuclei. This may be due to a higher vulnerability to thermal noise related to MRI system electronics, gradient switching artifact and physiological noise including cardiac pulsations and respiratory activity (Wang et al., 2014). This can be further investigated using 7T data, or multi-echo data, by testing whether this distinction remains in data where the subcortical signal to noise ratio is improved. Figs. 3 and 4 show that multiscale entropy curves, and their associated complexity indices, are considerably affected by the choice of the tolerance parameter r and embedding dimension m (see Omidvarnia et al., 2018 for another in-depth investigation of the role of r and m in sample entropy). As the bottom rows of the figures suggest, the *relative network ordering* of complexity indices is a consistent discriminative feature across RSNs. The effect size of complex signatures across RSNs decreases at smaller r's (note the difference between the upper and lower rows of Fig. 6) and at lower temporal resolutions (note the systematic reduction from left to right in Fig. 6). Having said that, almost all of pair-wise Hedges' g statistics remain statistically significant after bootstrapping (see Tables S6 and S7), also due to our large sample cohort. The embedding dimension m is an influential factor in multiscale entropy analysis which controls the dimensionality of the reconstructed phase space (Omidvarnia et al., 2018). For a given embedding dimension m, a tolerance r, and a single time scale τ, multiscale entropy estimates the average logarithm of the probability that if two segments of length m in the data are closer than r then two segments of length $m + 1$ also have a distance less than r. We tested a range of values for m throughout the study and found a consistent estimate of multiscale entropy for the tolerance parameter r=0.5 up to $m = 10$ and a severe loss of the estimates for r=0.15 for $m \geq 4$ at the original temporal resolution of rsfMRI, i.e., T_R=720 ms (Fig. 3 vs. Fig. 4). The mean RSN complexity indices in the lower rows of Fig. 5 as well as Figs. S1 to S3 suggest that at longer T_R's the embedding dimension above m=3 may reduce the separability of RSNs (in particular, as the tolerance parameter r=0.15). Since HCP datasets consist of four rsfMRI recording sessions per subject, we were in a good position to perform a test-retest analysis of network-specific multiscale entropy. Fig. S5 illustrates the finding in terms of two color-coded maps based on the intra-class correlation coefficient, a measure of reproducibility, extracted from network-specific sample entropy distributions at single time scales. As the figure suggests, sample entropy values over fine time scales ($\tau \leq 5$) are more repeatable than the values extracted at large scales. This finding was not surprising because coarse-graining step of the multiscale entropy analysis at large τ can remove original information from rsfMRI time series and reduce them into a series of random fluctuations.

The biological underpinnings of multiscale entropy has been subject to several studies in the recent years (e.g., Liu et al., 2019; McDonough and Nashiro, 2014; Wang et al., 2018b). Ghanbari et al. (2015) hypothesized that more predictable neural signals establish synchronized links between remote brain regions and, therefore, facilitate long-range information processing of functional brain networks. Also, increasingly random signals are related to the local firing of neural populations. This dichotomy has been also reported for coarse-fine time scales of multiscale entropy: fine scale values correspond to local information processing of brain networks, while coarse scale values deal with long-range communications (McDonough and Nashiro, 2014; McIntosh et al., 2014; Vakorin et al., 2011; Wang et al., 2018b). Functional brain connectivity may play an important role here. In fact, functional brain connectivity and temporal complexity of RSNs represent a scale-dependant relationship with a negative correlation at fine scales (small values of τ) and a positive correlation at coarse scales (large values of τ) McDonough and Nashiro (2014). Our results not only reinforce this finding (see Fig. 8), but also they suggest that the brain regions with highest mean temporal complexity are mainly located across the default mode network, frontoparietal network and dorsal attention network (see Fig. 7). These regions have also been reported as having high *participation coefficients* in the functional brain networks and therefore, playing as *connector nodes* in the brain (Bertolero et al., 2018; 2015). The overlap between the participation coefficient and temporal complexity brain maps may suggest a link between RSN complexity and integration of various cognitive functions in the brain. As Fig. 7 illustrates, the temporal complexity

patterns of rsfMRI are asymmetrical across the brain (e.g. frontal, temporal, and primary motor regions). This observation may be related to the lateralization of human brain organization and cognition (Witelson, 1988).

The impact of rsfMRI preprocessing has been subject to extensive research (see Esteban et al., 2019; Power et al., 2012; Yan and Zang, 2010; Zuo et al., 2013, for examples). However, there is still no complete agreement on the most appropriate rsfMRI preprocessing pipeline, as this depends on several factors such as the MRI scanner type, scanning parameters, subject-specific movement artifacts, health conditions and nature of the study (e.g., whether it is a resting state study or an event-related study). The rsfMRI datasets of this study were preprocessed using a customized pipeline for the HCP project that includes ICA-FIX (Glasser et al., 2013). There is evidence suggesting that ICA-FIX is robust in reducing artefacts in large rsfMRI datasets. That is why it has been the recommended rsfMRI preprocessing pipeline by the HCP because it allows for combined cortical surface and subcortical volume analysis (Glasser et al., 2013). Also, motion artefact removal using the ICA-FIX method (Griffanti et al., 2014; Salimi-Khorshidi et al., 2014) has been shown to result in significantly improved RSN reproducibility, regardless of the recording conditions (Pruim et al., 2015). The choice of brain parcellation is another impactful factor in the temporal complexity analysis of rsfMRI which defines the spatial extent and morphology of ROIs and RSNs. It is important to use non-overlapping brain parcels (e.g., the brain atlas (Glasser et al., 2016) used in tis study) for defining RSNs in order to avoid any interference of complex dynamics across brain regions. An example of an overlapping brain parcellation is the definition of ROIs based on principal components of brain function.

A limitation of multiscale entropy for temporal complexity analysis of functional brain networks originates from the general framework of sample and multiscale entropy analyses as univariate methods. This means that the input signal to these measures is always one-dimensional. In the context of this study, ROI-specific multiscale entropy patterns do not measure multivariate relationships between brain regions necessarily. Although we considered pair-wise relationships between the complexity distributions of RSNs (see Tables S6 and S7), it is not a substitute for multivariate complexity measures. It speaks to the necessity of developing multivariate versions of sample/multiscale entropy measures which can deal with a more global picture of dynamical brain function at once (for example, see Ahmed and Mandic, 2012).

5. Conclusion

Functional brain networks represent distinctive signatures of temporal complexity which can be quantified through multiscale entropy analysis of rsfMRI. This observation is robust over a large cohort of unrelated subjects and reproducible over rsfMRI recording sessions. Head motion has a significantly lower temporal complexity than RSNs. Also, there is likely a non-random correlation between temporal complexity of RSNs and higher-order cognition (fluid intelligence).

Disclosure of Competing Interest

The authors declare no conflict of interest.

Credit authorship contribution statement

Amir Omidvarnia: Conceptualization, Methodology, Software, Formal analysis, Validation, Writing - original draft. **Andrew Zalesky:** Conceptualization, Methodology, Validation, Writing - review & editing. **Sina Mansour L.:** Writing - review & editing. **Dimitri Van De Ville:** Conceptualization, Methodology, Validation, Writing - review & editing. **Graeme D. Jackson:** Conceptualization, Validation, Writing - review & editing. **Mangor Pedersen:** Conceptualization, Methodology, Validation, Writing - review & editing.

Acknowledgement

AO acknowledges financial support through the Eurotech Postdoc Program, co-funded by the European Commission under its framework program Horizon 2020 (Grant Agreement number 754462). This study was supported by the National Health and Medical Research Council (NHMRC) of Australia (no. 628952). The Florey Institute of Neuroscience and Mental Health acknowledges the strong support from the Victorian Government and in particular the funding from the Operational Infrastructure Support Grant. We also acknowledge the facilities, and the scientific and technical assistance of the National Imaging Facility (NIF) at the Florey node and The Victorian Biomedical Imaging Capability (VBIC). GJ is supported by an NHMRC practitioner's fellowship (no 1060312). The primary rsfMRI data in this study was provided by the Human Connectome Project, WUMinn Consortium (1U54MH091657; Principal Investigators: David Van Essen and Kamil Ugurbil) funded by the 16 National Institutes of Health (NIH) institutes and centers that support the NIH Blueprint for Neuroscience Research; and by the McDonnell Center for Systems Neuroscience at Washington University.

Supplementary material

Supplementary material associated with this article can be found, in the online version, at doi:10.1016/j.neuroimage.2021.117760.

References

Ahmed, M.U., Mandic, D.P., 2012. Multivariate multiscale entropy analysis. IEEE Signal Process. Lett. 19 (2), 91–94.

Allen, E.A., Damaraju, E., Plis, S.M., Erhardt, E.B., Eichele, T., Calhoun, V.D., 2012. Tracking whole-brain connectivity dynamics in the resting state. Cereb. Cortex 24 (3), 663–676. doi:10.1093/cercor/bhs352.

Barch, D.M., Burgess, G.C., Harms, M.P., Petersen, S.E., Schlaggar, B.L., Corbetta, M., Glasser, M.F., Curtiss, S., Dixit, S., Feldt, C., Nolan, D., Bryant, E., Hartley, T., Footer, O., Bjork, J.M., Poldrack, R., Smith, S., Johansen-Berg, H., Snyder, A.Z., Essen, D.C.V., 2013. Function in the human connectome: Task-fmri and individual differences in behavior. NeuroImage 80, 169–189. doi:10.1016/j.neuroimage.2013.05.033.

Bassett, D., Bullmore, E., 2006. Small-world brain networks. Neuroscientist 12 (6), 512–523.

Bassett, D., Gazzaniga, M., 2011. Understanding complexity in the human brain. Trends Cognit. Sci. 15 (5), 200–209.

Bassett, D., Nelson, B., Mueller, B., Camchong, J., Lim, K., 2012. Altered resting state complexity in schizophrenia. Neuroimage 59 (3), 2196–2207.

Beckmann, C.F., DeLuca, M., Devlin, J.T., Smith, S.M., 2005. Investigations into resting-state connectivity using independent component analysis. Philos. Trans. R. Soc. B 360 (1457), 1001–1013. doi:10.1098/rstb.2005.1634.

Bertolero, M.A., Yeo, B.T., Bassett, D.S., D'Esposito, M., 2018. A mechanistic model of connector hubs, modularity and cognition. Nat. Hum. Behav. 2 (10), 765–777. doi:10.1038/s41562-018-0420-6.

Bertolero, M.A., Yeo, B.T.T., D'Esposito, M., 2015. The modular and integrative functional architecture of the human brain. Proceedings of the National Academy of Sciences 112 (49), E6798–E6807. doi:10.1073/pnas.1510619112. https://www.pnas.org/content/112/49/E6798.full.pdf

Biswal, B., Yetkin, F., Haughton, V., Hyde, J., 1995. Functional connectivity in the motor cortex of resting human brain using echo-planar MRI. Magn. Reson. Med. 34 (4), 537–541.

Britz, J., Ville, D.V.D., Michel, C.M., 2010. Bold correlates of eeg topography reveal rapid resting-state network dynamics. NeuroImage 52 (4), 1162–1170. doi:10.1016/j.neuroimage.2010.02.052.

Brown, C., Jiang, Y., Smith, C., Gold, B., 2018. Age and Alzheimer's pathology disrupt default mode network functioning via alterations in white matter microstructure but not hyperintensities. Cortex 104, 58–74.

Caspers, S., Eickhoff, S.B., Geyer, S., Scheperjans, F., Mohlberg, H., Zilles, K., Amunts, K., 2008. The human inferior parietal lobule in stereotaxic space. Brain Struc. Funct. 212 (6), 481–495. doi:10.1007/s00429-008-0195-z.

Cattell, R.B., 1963. Theory of fluid and crystallized intelligence: acritical experiment. J. Educ. Psychol. 54 (1), 1–22. doi:10.1037/h0046743.

Chang, C., Glover, G.H., 2010. Time-frequency dynamics of resting-state brain connectivity measured with FMRI. NeuroImage 50 (1), 81–98. doi:10.1016/j.neuroimage.2009.12.011.

Cherkassky, V.L., Kana, R.K., Keller, T.A., Just, M.A., 2006. Functional connectivity in a baseline resting-state network in autism. Neuroreport 17 (16), 1687–1690. doi:10.1097/01.wnr.0000239956.45448.4c.

Costa, M., Goldberger, A., 2015. Generalized multiscale entropy analysis: Application to quantifying the complex volatility of human heartbeat time series. Entropy 17 (3), 1197–1203. doi:10.3390/e17031197.

Costa, M., Goldberger, A., Peng, C., 2002. Multiscale entropy analysis of complex physiologic time series. Phys. Rev. Lett. 89 (6), 068102.
Costa, M., Goldberger, A.L., Peng, C.-K., 2005. Multiscale entropy analysis of biological signals. Phys. Rev. E 71, 021906. doi:10.1103/PhysRevE.71.021906.
Draper, N., Smith, H., 1967. Applied Regression Analysis, by N.R. Draper and H. Smith. John Wiley and Sons.
Esteban, O., Markiewicz, C.J., Blair, R.W., Moodie, C.A., Isik, A.I., Erramuzpe, A., Kent, J.D., Goncalves, M., DuPre, E., Snyder, M., Oya, H., Ghosh, S.S., Wright, J., Durnez, J., Poldrack, R.A., Gorgolewski, K.J., 2019. fMRIPrep: a robust preprocessing pipeline for functional MRI. Nature Methods 16 (1), 111–116. doi:10.1038/s41592-018-0235-4.
Fischl, B., Stevens, A.A., Rajendran, N., Yeo, B.T.T., Greve, D.N., Van Leemput, K., Polimeni, J.R., Kakunoori, S., Buckner, R.L., Pacheco, J., Salat, D.H., Melcher, J., Frosch, M.P., Hyman, B.T., Grant, P.E., Rosen, B.R., van der Kouwe, A.J.W., Wiggins, G.C., Wald, L.L., Augustinack, J.C., 2009. Predicting the location of entorhinal cortex from MRI. NeuroImage 47 (1), 8–17. doi:10.1016/j.neuroimage.2009.04.033.
Fox, M.D., Snyder, A.Z., Vincent, J.L., Corbetta, M., Van Essen, D.C., Raichle, M.E., 2005. The human brain is intrinsically organized into dynamic, anticorrelated functional networks. Proceedings of the National Academy of Sciences 102 (27), 9673–9678. doi:10.1073/pnas.0504136102. https://www.pnas.org/content/102/27/9673.full.pdf
Gao, Y., Zheng, J., Li, Y., Guo, D., Wang, M., Cui, X., Ye, W., 2018. Abnormal default--mode network homogeneity in patients with temporal lobe epilepsy. Medicine 97 (26), e11239.
Ghanbari, Y., Bloy, L., Christopher Edgar, J., Blaskey, L., Verma, R., Roberts, T.P.L., 2015. Joint analysis of band-specific functional connectivity and signal complexity in autism. J. Autism Dev. Disord. 45 (2), 444–460. doi:10.1007/s10803-013-1915-7.
Glasser, M.F., Coalson, T.S., Robinson, E.C., Hacker, C.D., Harwell, J., Yacoub, E., Ugurbil, K., Andersson, J., Beckmann, C.F., Jenkinson, M., Smith, S.M., Van Essen, D.C., 2016. A multi-modal parcellation of human cerebral cortex. Nature 536 (7615), 171–178. doi:10.1038/nature18933.
Glasser, M.F., Sotiropoulos, S.N., Wilson, J.A., Coalson, T.S., Fischl, B., Andersson, J.L., Xu, J., Jbabdi, S., Webster, M., Polimeni, J.R., Essen, D.C.V., Jenkinson, M., 2013. The minimal preprocessing pipelines for the human connectome project. NeuroImage 80, 105–124. doi:10.1016/j.neuroimage.2013.04.127.
Goldberger, A., Rigney, D., West, B., Goldberger, A., 1990. Chaos and fractals in human physiology. Sci. Am. 262 (2), 42–49.
Goldberger, A.L., 1996. Non-linear dynamics for clinicians: chaos theory, fractals, and complexity at the bedside. Lancet 347 (9011), 1312–1314.
Greicius, M.D., Flores, B.H., Menon, V., Glover, G.H., Solvason, H.B., Kenna, H., Reiss, A.L., Schatzberg, A.F., 2007. Resting-state functional connectivity in major depression: abnormally increased contributions from subgenual cingulate cortex and Thalamus. Biol. Psychiatry 62 (5), 429–437. doi:10.1016/j.biopsych.2006.09.020.
Griffanti, L., Salimi-Khorshidi, G., Beckmann, C.F., Auerbach, E.J., Douaud, G., Sexton, C.E., Zsoldos, E., Ebmeier, K.P., Filippini, N., Mackay, C.E., Moeller, S., Xu, J., Yacoub, E., Baselli, G., Ugurbil, K., Miller, K.L., Smith, S.M., 2014. ICA-based artefact removal and accelerated fMRI acquisition for improved resting state network imaging. NeuroImage 95, 232–247. doi:10.1016/j.neuroimage.2014.03.034.
Hawrylycz, M.J., Lein, E.S., Guillozet-Bongaarts, A.L., Shen, E.H., Ng, L., Miller, J.A., van de Lagemaat, L.N., Smith, K.A., Ebbert, A.J., Riley, Z.L., Abajian, C., Beckmann, C.F., Bernard, A., Bertagnolli, D., Boe, A.F., Cartagena, P.M., Chakravarty, M.M., Chapin, M., Chong, J., Dalley, R.A., Daly, B.D., Dang, C., Datta, S., Dee, N., Dolbeare, T., Faber, V., Feng, D., Fowler, D.R., Goldy, J., Gregor, B.W., Haradon, Z., Haynor, D.R., Hohmann, J.G., Horvath, S., Howard, R.E., Jeromin, A., Jochim, J.M., Kinnunen, M., Lau, C.D., Lazarz, E.T., Lee, C., Lemon, T.A., Li, L., Li, Y., Morris, J.A., Overly, C.C., Parker, P.D., Parry, S.E., Reding, M., Royall, J.J., Schulkin, J., Sequeira, P.A., Slaughterbeck, C.R., Smith, S.C., Sodt, A.J., Sunkin, S.M., Swanson, B.E., Vawter, M.P., Williams, D.S., Wohnoutka, P.E., Zielke, H.R., Geschwind, D.H., Hof, P.R., Smith, S.M., Koch, C., Grant, S.G.N., Jones, A.R., 2012. An anatomically comprehensive atlas of the adult human brain transcriptome. Nature 489, 391–399.
Hedges, L.V., 1981. Distribution theory for glass's estimator of effect size and related estimators. J. Educ. Stat. 6 (2), 107–128.
Hentschke, H., Stüttgen, M.C., 2011. Computation of measures of effect size for neuroscience data sets.. Eur. J. Neurosci. 34 12, 1887–1894.
van den Heuvel, M., Hulshoff Pol, H., 2010. Exploring the brain network: a review on resting-state FMRI functional connectivity. Eur. Neuropsychopharmacol. 20 (8), 519–534. doi:10.1016/j.euroneuro.2010.03.008.
Hodkinson, D.J., Krause, K., Khawaja, N., Renton, T.F., Huggins, J.P., Vennart, W., Thacker, M.A., Mehta, M.A., Zelaya, F.O., Williams, S.C., Howard, M.A., 2013. Quantifying the test-retest reliability of cerebral blood flow measurements in a clinical model of on-going post-surgical pain: astudy using pseudo-continuous arterial spin labelling. NeuroImage 3, 301–310. doi:10.1016/j.nicl.2013.09.004.
Hutchison, R., Womelsdorf, T., Allen, E., Bandettini, P., Calhoun, V., Corbetta, M., Della Penna, S., Duyn, J., Glover, G., Gonzalez-Castillo, J., Handwerker, D., Keilholz, S., Kiviniemi, V., Leopold, D., de Pasquale, F., Sporns, O., Walter, M., Chang, C., 2013. Dynamic functional connectivity: promise, issues, and interpretations.
Kirst, C., Timme, M., Battaglia, D., 2016. Dynamic information routing in complex networks. Nat. Commun. 7.
Laufs, H., Tagliazucchi, E., von Wegner, F., Jahnke, K., Morzelewski, A., Borisov, S., Steinmetz, H., 2012. Influence of vigilance on resting state brain activity. Klin Neurophysiol. 43, V150.
Liu, M., Song, C., Liang, Y., Knöpfel, T., Zhou, C., 2019. Assessing spatiotemporal variability of brain spontaneous activity by multiscale entropy and functional connectivity. NeuroImage 198, 198–220. doi:10.1016/j.neuroimage.2019.05.022.
Liu, X., Duyn, J.H., 2013. Time-varying functional network information extracted from brief instances of spontaneous brain activity. Proceedings of the National Academy of Sciences 110 (11), 4392–4397. doi:10.1073/pnas.1216856110. https://www.pnas.org/content/110/11/4392.full.pdf
Liégeois, R., Li, J., Kong, R., Orban, C., Van De Ville, D., Ge, T., Sabuncu, M.R., Yeo, B.T.T., 2019. Resting brain dynamics at different timescales capture distinct aspects of human behavior. Nat. Commun. 10 (1), 2317. doi:10.1038/s41467-019-10317-7.
Lynn, C.W., Bassett, D.S., 2018. The physics of brain network structure, function and control. Nat. Rev. Phys. 1, 318–332.
Maxim, V., Şendur, L., Fadili, J., Suckling, J., Gould, R., Howard, R., Bullmore, E., 2005. Fractional gaussian noise, functional MRI and Alzheimer's disease. NeuroImage 25 (1), 141–158. doi:10.1016/j.neuroimage.2004.10.044.
McDonough, I., Nashiro, K., 2014. Network complexity as a measure of information processing across resting-state networks: evidence from the human connectome project. Front. Hum. Neurosci. 8, 409. doi:10.3389/fnhum.2014.00409.
McIntosh, A., Vakorin, V., Kovacevic, N., Wang, H., Diaconescu, A., Protzner, A., 2014. Spatiotemporal dependency of age-related changes in brain signal variability. Cereb. Cortex 24 (7), 1806–1817.
McIntosh, A.R., Kovacevic, N., Itier, R.J., 2008. Increased brain signal variability accompanies lower behavioral variability in development. PLoS Comput. Biol. 4 (7), 1–9. doi:10.1371/journal.pcbi.1000106.
Mišić, B., Vakorin, V.A., Paus, T., McIntosh, A.R., 2011. Functional embedding predicts the variability of neural activity. Front. Syst. Neurosci. 5. doi:10.3389/fnsys.2011.00090.
Niu, Y., Wang, B., Zhou, M., Xue, J., Shapour, H., Cao, R., Cui, X., Wu, J., Xiang, J., 2018. Dynamic complexity of spontaneous bold activity in alzheimer's disease and mild cognitive impairment using multiscale entropy analysis. Front. Neurosci. 12, 677. doi:10.3389/fnins.2018.00677.
Ohta, M., Nakataki, M., Takeda, T., Numata, S., Tominaga, T., Kameoka, N., Kubo, H., Kinoshita, M., Matsuura, K., Otomo, M., Takeichi, N., Harada, M., Ohmori, T., 2018. Structural equation modeling approach between salience network dysfunction, depressed mood, and subjective quality of life in schizophrenia: an ICA resting-state fMRI study. Neuropsychiatr. Dis. Treat. 14, 1585–1597.
Omidvarnia, A., Mesbah, M., Pedersen, M., Jackson, G., 2018. Range entropy: a bridge between signal complexity and self-similarity. Entropy 20 (12). doi:10.3390/e20120962.
Omidvarnia, A., Pedersen, M., Walz, J.M., Vaughan, D.N., Abbott, D.F., Jackson, G.D., 2016. Dynamic regional phase synchrony (dreps). Hum. Brain Map. 37 (5), 1970–1985. doi:10.1002/hbm.23151.
Park, H.-J., Friston, K., 2013. Structural and functional brain networks: from connections to cognition. Science 342 (6158). doi:10.1126/science.1238411.
Pedersen, M., Omidvarnia, A., Walz, J., Zalesky, A., Jackson, G., 2017. Spontaneous brain network activity: analysis of its temporal complexity. Netw. Neurosci. 1 (2), 100–115.
Pedersen, M., Omidvarnia, A., Zalesky, A., Jackson, G.D., 2018. On the relationship between instantaneous phase synchrony and correlation-based sliding windows for time-resolved FMRIconnectivity analysis. NeuroImage 181, 85–94. doi:10.1016/j.neuroimage.2018.06.020.
Power, J.D., Barnes, K.A., Snyder, A.Z., Schlaggar, B.L., Petersen, S.E., 2012. Spurious but systematic correlations in functional connectivity MRI networks arise from subject motion. NeuroImage 59 (3), 2142–2154. doi:10.1016/j.neuroimage.2011.10.018.
Power, J.D., Mitra, A., Laumann, T.O., Snyder, A.Z., Schlaggar, B.L., Petersen, S.E., 2014. Methods to detect, characterize, and remove motion artifact in resting state FMRI. NeuroImage 84, 320–341. doi:10.1016/j.neuroimage.2013.08.048.
Preti, M.G., Bolton, T.A., Ville, D.V.D., 2017. The dynamic functional connectome: State-of-the-art and perspectives. NeuroImage 160, 41–54. doi:10.1016/j.neuroimage.2016.12.061.
Pruim, R.H., Mennes, M., Buitelaar, J.K., Beckmann, C.F., 2015. Evaluation of ICA-aroma and alternative strategies for motion artifact removal in resting state FMRI. NeuroImage 112, 278–287. doi:10.1016/j.neuroimage.2015.02.063.
Richiardi, J., Achard, S., Bunke, H., Ville, D.V.D., 2013. Machine learning with brain graphs: predictive modeling approaches for functional imaging in systems neuroscience. IEEE Signal Process. Mag. 30, 58–70.
Richiardi, J., Eryilmaz, H., Schwartz, S., Vuilleumier, P., Ville, D.V.D., 2011. Decoding brain states from FMRI connectivity graphs. NeuroImage 56, 616–626.
Richman, J., Moorman, J., 2000. Physiological time-series analysis using approximate entropy and sample entropy. Am. J. Physiol. Heart Circ. Physiol. 278 (6), H2039–2049.
Salimi-Khorshidi, G., Douaud, G., Beckmann, C.F., Glasser, M.F., Griffanti, L., Smith, S.M., 2014. Automatic denoising of functional MRI data: combining independent component analysis and hierarchical fusion of classifiers. NeuroImage 90, 449–468. doi:10.1016/j.neuroimage.2013.11.046.
Seeley, W.W., Menon, V., Schatzberg, A.F., Keller, J., Glover, G.H., Kenna, H., Reiss, A.L., Greicius, M.D., 2007. Dissociable intrinsic connectivity networks for salience processing and executive control. J. Neurosci. 27 (9), 2349–2356. doi:10.1523/JNEUROSCI.5587-06.2007.
Shen, H., Li, Z., Qin, J., Liu, Q., Wang, L., Zeng, L.-L., Li, H., Hu, D., 2016. Changes in functional connectivity dynamics associated with vigilance network in taxi drivers. NeuroImage 124, 367–378. doi:10.1016/j.neuroimage.2015.09.010.
Shine, J.M., Breakspear, M., Bell, P.T., Ehgoetz Martens, K.A., Shine, R., Koyejo, O., Sporns, O., Poldrack, R.A., 2019. Human cognition involves the dynamic integration of neural activity and neuromodulatory systems. Nat. Neurosci. 22 (2), 289–296. doi:10.1038/s41593-018-0312-0.
Shrout, P.E., Fleiss, J.L., 1979. Intraclass correlations: uses in assessing rater reliability.. Psychol. Bull. 86 2, 420–428.
Sokunbi, M., Gradin, V., Waiter, G., Cameron, G., Ahearn, T., Murray, A., Steele, D., Staff, R., 2014. Nonlinear complexity analysis of brain FMRI signals in schizophrenia. PLoS One 9 (5), 1–10. doi:10.1371/journal.pone.0095146.
Tagliazucchi, E., Von Wegner, F., Morzelewski, A., Brodbeck, V., Laufs, H., 2012. Dynamic bold functional connectivity in humans and its electrophysiological correlates. Front. Hum. Neurosci. 6, 339. doi:10.3389/fnhum.2012.00339.

Thompson, W., Brantefors, P., Fransson, P., 2017. From static to temporal network theory: applications to functional brain connectivity. Netw. Neurosci. 1 (2), 69–99.

Vakorin, V.A., Lippé, S., McIntosh, A.R., 2011. Variability of brain signals processed locally transforms into higher connectivity with brain development. Journal of Neuroscience 31 (17), 6405–6413. doi:10.1523/JNEUROSCI.3153-10.2011. https://www.jneurosci.org/content/31/17/6405.full.pdf.

Valverde, S., Ohse, S., Turalska, M., West, B.J., Garcia-Ojalvo, J., 2015. Structural determinants of criticality in biological networks. Front. Physiol. 6, 127. doi:10.3389/fphys.2015.00127.

Van De Ville, D., Britz, J., Michel, C.M., 2010. Eeg microstate sequences in healthy humans at rest reveal scale-free dynamics. Proceedings of the National Academy of Sciences 107 (42), 18179–18184. doi:10.1073/pnas.1007841107.

Van Essen, D.V., Ugurbil, K., Auerbach, E., Barch, D., Behrens, T., Bucholz, R., Chang, A., Chen, L., Corbetta, M., Curtiss, S., Penna, S.D., Feinberg, D., Glasser, M., Harel, N., Heath, A., Larson-Prior, L., Marcus, D., Michalareas, G., Moeller, S., Oostenveld, R., Petersen, S., Prior, F., Schlaggar, B., Smith, S., Snyder, A., Xu, J., Yacoub, E., 2012. The human connectome project: A data acquisition perspective. NeuroImage 62 (4), 2222–2231. doi:10.1016/j.neuroimage.2012.02.018.

Wang, D., Jann, K., Fan, C., Qiao, Y., Zang, Y., Lu, H., Yang, Y., 2018. Neurophysiological basis of multi-scale entropy of brain complexity and its relationship with functional connectivity. Front. Neurosci. 12, 352.

Wang, D.J.J., Jann, K., Fan, C., Qiao, Y., Zang, Y.-F., Lu, H., Yang, Y., 2018. Neurophysiological basis of multi-scale entropy of brain complexity and its relationship with functional connectivity. Front. Neurosci. 12. doi:10.3389/fnins.2018.00352.

Wang, Z., Li, Y., Childress, A.R., Detre, J.A., 2014. Brain entropy mapping using FMRI. PLoS One 9 (3), 1–8. doi:10.1371/journal.pone.0089948.

Weng, W.-C., Jiang, G.J.A., Chang, C.-F., Lu, W.-Y., Lin, C.-Y., Lee, W.-T., Shieh, J.-S., 2015. Complexity of multi-channel electroencephalogram signal analysis in childhood absence epilepsy. PLoS One 10 (8), 1–14. doi:10.1371/journal.pone.0134083.

Witelson, S.F., 1988. Brain asymmetry, functional aspects. In: Hobson, J.A. (Ed.), States of Brain and Mind. Birkhäuser, Boston, MA, pp. 13–16. doi:10.1007/978-1-4899-6771-8_6.

Wong, C.W., Olafsson, V.T., Tal, O., Liu, T.T., 2013. The amplitude of the resting-state FMRI global signal is related to eeg vigilance measures. NeuroImage 83, 983–990.

Yan, C., Zang, Y., 2010. Dparsf: a matlab toolbox for ”pipeline” data analysis of resting-state FMRI. Front. Syst. Neurosci. 4, 13. doi:10.3389/fnsys.2010.00013.

Yang, A.C., Tsai, S.-J., Yang, C.-H., Kuo, C.-H., Chen, T.-J., Hong, C.-J., 2011. Reduced physiologic complexity is associated with poor sleep in patients with major depression and primary insomnia. J. Affect. Disord. 131 (1), 179–185. doi:10.1016/j.jad.2010.11.030.

Yeo, B.T., Krienen, F.M., Sepulcre, J., Sabuncu, M.R., Lashkari, D., Hollinshead, M., Roffman, J.L., Smoller, J.W., Zöllei, L., Polimeni, J.R., Fischl, B., Liu, H., Buckner, R.L., 2011. The organization of the human cerebral cortex estimated by intrinsic functional connectivity. J. Neurophysiol. 106 (3), 1125–1165. doi:10.1152/jn.00338.2011.

Zalesky, A., Fornito, A., Cocchi, L., Gollo, L.L., Breakspear, M., 2014. Time-resolved resting-state brain networks. Proceedings of the National Academy of Sciences 111 (28), 10341–10346. doi:10.1073/pnas.1400181111.

Zuo, X.-N., Xu, T., Jiang, L., Yang, Z., Cao, X.-Y., He, Y., Zang, Y.-F., Castellanos, F.X., Milham, M.P., 2013. Toward reliable characterization of functional homogeneity in the human brain: preprocessing, scan duration, imaging resolution and computational space. NeuroImage 65, 374–386. doi:10.1016/j.neuroimage.2012.10.017.